Journal of Composites Science

MDPI

Article

Temperature Study during the Edge Trimming of Carbon Fiber-Reinforced Plastic $[0]_8$/Ti6Al4V Stack Material

Arquimedes Castillo-Morales [1], Xavier Rimpault [1], Jean-François Chatelain [1,*] and Gilbert Lebrun [2]

[1] Department of Mechanical Engineering, École de Technologie Supérieure de Montréal, 1100 Notre-Dame Street West, Montreal, QC H3C 1K3, Canada; arquimedes.castillo-morales.1@ens.etsmtl.ca (A.C.-M.); cc-xavier.rimpault@etsmtl.ca (X.R.)

[2] Department of Mechanical Engineering, Université du Québec à Trois-Rivières, 3351 Boul. des Forges, Trois-Rivières, QC G9A 5H7, Canada; gilbert.lebrun@uqtr.ca

* Correspondence: jean-francois.chatelain@etsmtl.ca

Abstract: Carbon Fiber-Reinforced Plastic (CFRP) and Titanium alloy (Ti6Al4V) stacks are used extensively in the modern aerospace industry thanks to their outstanding mechanical properties and resistance to thermal load applications. Machining the CFRP/Ti6Al4V stack is a challenge and is complicated by the differences in each constituent materials' machinability. The difficulty arises from the matrix degradation of the CFRP material caused by the heat generated during the machining process, which is a consequence of the low thermal conductivity of Ti6Al4V material. In most cases, CFRP and Ti6Al4V materials are stacked and secured together using rivets or bolts. This results in extra weight, while the drilling process required for such an assembly may damage the CFRP material. To overcome these issues, some applications employ an assembly that is free of bolts or rivets, and which uses adhesives or an adapted curing process to bond both materials together. The present research analyzes a thermal distribution and its effect on quality during the edge trimming process of a CFRP/Ti6Al4V stack assembly. Different types of tools and cutting parameters are compared using thermocouples embedded within the material and others on the tool cutting edge. In contrast to previous studies, the feed rate was the most significant factor affecting the cutting temperature and quality of the workpiece, while the cutting speed had no significant impact. The temperature in the workpiece increases as the feed per tooth decreases.

Keywords: multimaterial stack machining; fiber-reinforced plastic; titanium alloy; trimming; thermal analysis; thermocouples

Citation: Castillo-Morales, A.; Rimpault, X.; Chatelain, J.-F.; Lebrun, G. Temperature Study during the Edge Trimming of Carbon Fiber-Reinforced Plastic $[0]_8$/Ti6Al4V Stack Material. *J. Compos. Sci.* **2021**, *5*, 137. https://doi.org/10.3390/jcs5050137

Academic Editors: Michela Simoncini, Thanasis Triantafillou and Francesco Tornabene

Received: 7 April 2021
Accepted: 17 May 2021
Published: 19 May 2021

1. Introduction

Military and commercial industries are always seeking to decrease fuel consumption by reducing aircraft structural components' weight. Carbon Fiber-Reinforced Plastic (CFRP) and Titanium grade 5 (Ti6Al4V) material stacks are commonly used in airframe component assemblies thanks to their mechanical properties, such as a high strength-to-weight ratio and an excellent resistance to corrosion and fatigue [1]. These properties are leveraged as CFRP/Ti6Al4V material stacks are used to manufacture aircraft structures subjected to high thermo-mechanical stresses. An example of this use can be seen in the wing-fuselage connection of the new-generation Boeing 787 Dreamliner [1].

Generally, CFRP/Ti6Al4V material stacks are assembled using rivets or bolts, in which case the CFRP and the Ti plaques are trimmed individually and then stacked up to enhance the required tolerances. However, with specific requirements or applications, both plaques need to be bonded with adhesives or the composite cured with titanium, after which the plaques are trimmed together up to their final shape. This is because CFRP is very sensitive to notch or delamination resulting from drilling, which may severely decrease the component's mechanical properties in service.

Several publications focus on the trimming of CFRP and Ti6Al4V individually, while in the case of CFRP/Ti6Al4V stacked together, most research works focus on the optimization of the drilling process [1–4] and on cutting force analysis and modelling [5,6]. Regarding the edge milling of such material stacks, the literature contains relatively little information regarding thermal analysis or machining temperature studies. Since the machining temperature during CFRP/Ti6Al4V trimming plays a crucial role in avoiding reaching the CFRP's glass transition temperature, this research investigates the temperature distribution during the trimming of CFRP/Ti6Al4V stacks.

1.1. Temperature Measurement Methods

Although most of the works covering the trimming of CFRP and Ti6Al4V deal with the optimization of cutting parameters, studies also focus on the effect of these cutting parameters on the temperature at the tool–material interface during the cutting process. Generally, infrared cameras are used to measure the temperature in static bodies, although some studies have used them to measure the temperature at cutting high speed during the end mill cutting processes, pointing out measurements at both cutting tool and workpiece [7,8]. However, in the latter, thermography images were found to be inaccurate due to heat saturation on the primary shear zone and some areas hidden by the cutter body. More recently, Sheikh-Ahmad et al. [9] used the black body technique, which consists of heating each body to the same temperature to know the emissivity of each one, resulting in a detailed and contrasted thermography image. Nevertheless, in that study, the emissivity was measured with both objects in a fixed state, causing the emissivity values to change when the cutter rotated and moved forward. Another technique applied to metal cutting is the tool–workpiece thermocouple method, which uses embedded thermocouples both in the workpiece and at the tool edges. For the workpiece, thermocouples are embedded between CFRP layers [7], in holes [9], or handicraft-type thermocouples [10–12]. On the other hand, the temperature on the cutting tool can be measured by sticking thermocouples on the cutter tip [3] or through voltage differences between the workpiece and the cutter [7]. Although the tool–workpiece thermocouple method performed well during the milling process, parasite temperature estimation was reported due to the low stiffness of the setup in the case of Ti6Al4V machining [13] or due to thermocouple displacement during the CFRP lay-up [7]. Another application method consists in using a telemetry system that transmits the signal from thermocouple through the tool holder to a Transducer Via Wireless (TVW) transmission [14–18]. A long and complex wiring connection from the cutter to the acquisition system is then avoided, although the TVW induces a time delay resulting in a sensitivity reduction [17].

1.2. Influence of the Machining Process of CFRP and Titanium on Cutting Temperature

Unlike the machining of metallic materials, for which the material removal mechanism is done through plastic deformation and material shearing, the chip formation mechanism during the machining of fiber-reinforced plastics (FRP) proceeds through brittle fracturing of the composite fibers. However, in both cases the energy involved in the cutting process is converted into heat. Therefore, the main source of heat is located in the primary shear zone at the tool–chip interface. Machining both materials together is challenging since the epoxy matrix of the CFRP component is damaged at cutting temperatures of about 185 °C (glass temperature transition, Tg), while the titanium material may reach temperatures above 500 °C in dry cutting conditions [10]. Moreover, the thermal conductivity λ of the Ti6Al4V can vary from 6 to 9 W/m.K [19,20], while the CFRP's longitudinal thermal conductivity is 6 W/m.K and its transversal thermal conductivity is 0.5 W/m.K [21], which is very low compared to titanium alloy.

It is well known that the machining temperature is influenced by the cutting parameters, the cutting tool technology used and the material properties of the workpiece. Moreover, numerical simulations have been used to study the temperature of the tool–chip interface during the Ti6Al4V milling process [19,22–24], although these do not describe the effects of the cutting parameters on the cutting temperature. Li et al. [13] studied the effects of the cutting speed on the cutting edge and workpiece temperature of Ti6Al4V during the milling process, and found that the heat generation increases with the cutting speed. Wu et al. analyzed [25] the effects of up- and down-milling on the tooltip temperature in the machining of Ti6Al4V alloy and found a higher temperature using down-milling. Pan et al. [26] developed a predictive cutting temperature model to calculate the impact of the cutting speed, the feed rate, and the axial depth of cut during the milling of Ti6Al4V using PolyCrystalline Diamond tools (PCD). The results showed that all three parameters used in the experiment affect the cutting temperature. Yujing et al. [10,27] studied the effects of the cutting speed, the feed rate, and the radial and axial depths of cut on the temperature at the Ti6Al4V-cutter interface by using a semi-artificial thermocouple. The analysis found that both the cutter and workpiece temperatures rise with the cutting speed, and to a lower extent with the feed rate as well. In the CFRP machining case, Yashiro et al. [7] studied the milling cutting temperature for both the cutter and workpiece using the tool–workpiece thermocouple method. From the analysis, a high cutting speed of up to 300 m/min is recommended to reduce the workpiece temperature. Haijin et al. [11] studied the effects of the cutting parameters on the forces and the temperature during the CFRP trimming. The greater the cutting speed, the lower the cutting forces; however, for the cutting temperature, the opposite is true. This is because the temperature increases at a notably higher rate as the cutting speed increases; this is explained by the fact that the cutting speed increase is the key factor affecting the temperature, while the feed rate affects the cutting forces. Additionally, Wang et al. [12] studied the thermal effects on the fiber orientation. They found that the temperature within the fiber increases with the cutting speed. They equally found that the lowest temperature is always observed for a laminate having a 45° fiber orientation with respect to the feed direction, while the highest temperature is observed for a laminate having a 135° fiber orientation, irrespective of the cutting speed. This is in agreement with the results previously found for the surface roughness of trimmed parts [28]. Kerrigan et al. [16] measured the cutter temperature by using the TVW during CFRP edge trimming, and found that the feed rate is the most significant factor affecting the cutter temperature. Even though there is a thermal camera to assess the workpiece temperature, the analysis does not report its temperature. More recently, Sheikh-Ahmad et al. [9] studied the heat flux surrounding the CFRP workpiece, chip, and cutting tool during edge trimming. The study showed that the highest temperature was located on the cutter, where it reached 220 to 250 °C, followed by the chip, where temperatures reached 160 to 220 °C. The workpiece was the coldest, with a temperature reaching about 60 °C. Neither the cutting speed nor the feed rate had a statistically significant effect on the temperature of the cutter. However, the feed rate was found to have a statistically significant impact on the workpiece temperature, with lower temperatures seen on the workpiece at higher feed rates, due to the shorter interaction between the cutter and the workpiece with increased feed rates.

This research aims to study the machining temperature distribution within both components of the CFRP/Ti6Al4V stack, considering different cutting tool geometries and cutting parameters. The interactions of these on the cutting forces, surface finish, and tool wear were analyzed.

2. Experimental Methodology and Setup

2.1. Cutting Tools

Three different 12.7 mm-diameter tools were chosen to trim CFRP/Ti6Al4V coupons to compare their tool wear and their impact on the cutting temperature, the cutting forces, and the roughness parameters of the resulting machined surface (tool specifications shown in Table 1). The Design of Experiment (DoE) was prepared and carried out after performing screening tests to find a common cutting range for the different cutters (Table 2). The DoE was a three-level full factorial, including a total of 45 experiments: there were 18 tests using tool1, 18 using tool2, and only 9 using tool3, since the latter could not sustain a 4 mm width of cut.

2). The DoE was a three-level full factorial, including a total of 45 experiments: there were 18 tests using tool1, 18 using tool2, and only 9 using tool3, since the latter could not sustain a 4 mm width of cut.

Table 1. Specifications of the cutting tools.

Cutter	Material	Cutting Flute		Geometry
Tool1 (N)	Uncoated solid carbide	Helix flute	4 flutes β = 30°	
Tool2 (W)	TiAlN+ TiAl-coated carbide	Helix flute	4 flutes β = 35°/38°	
Tool3 (O)	PCD	Straight flute	2 flutes β = −3°/0°	

Table 2. Level values for each plan of experiments' variable.

Level	v (m/min)	f_t (mm/tooth)	a_e (mm)
1	50	0.05	1
2	175	0.15	4.3
3	300	0.25	

2.2. Manufacturing Process of the CFRP/Ti6Al4V Coupons

The CFRP/Ti6Al4V test coupons used during the edge trimming experiments had the following dimensions: 102 mm (4 in) length, 51 mm (2 in) width, and 9 mm (23/64 in) thickness. The thickness result from the Ti6Al4V plaque, which was 3.2 mm (1/8 in), and the CFRP plaque, which was 5.8 mm (15/64 in). This corresponds to the typical thickness for such material stacks in the aeronautical industry [29]. The $[0]_8$ CFRP plaque was made of a balanced carbon-epoxy prepreg CYCOM® 5320-1 T650-35 3K 8HS fabric 36%, which had a thread count of 24 × 1 picks/inch in the warp and weft directions. The resulting fiber volume fraction (V_f) was 56%, while the epoxy's glass transition was 190 °C. Ten thermocouples (TFCY-003, Chromega®-TFAL-003, Alomega® type K) were embedded within the stack on both sides of each coupon, in order to have results related to the two widths of cut investigated (a_e = 1.5 mm and a_e = 5 mm) along a 102 mm length of each coupon (Figure 1a). As shown, four thermocouples were welded (Vishay model 700® micro-welding machine) on the Titanium plaque, while six were embedded between plies of the CFRP (Figure 1b) to obtain the thermocouple distribution within the $[0]_8$/Ti6Al4V stack.

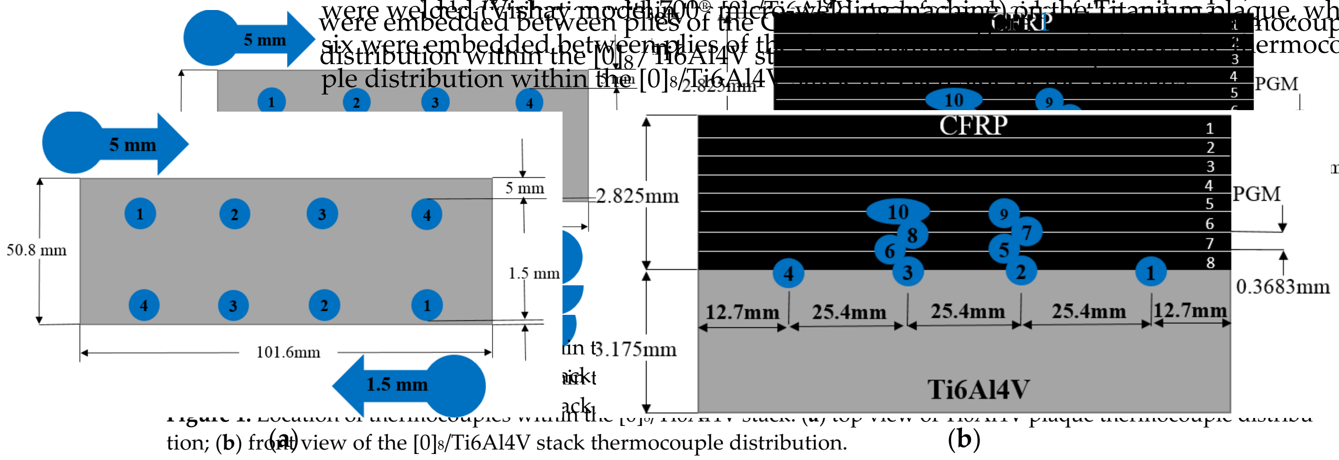

Figure 1. Location of thermocouples within the $[0]_8$/Ti6Al4V stack: (**a**) top view of Ti6Al4V plaque thermocouple distribution; (**b**) front view of the $[0]_8$/Ti6Al4V stack thermocouple distribution.

Both materials were assembled with the prepreg curing cycle to bond the CFRP plies to the Ti6Al4V plaque using the TAD2-52-1E oven (Despatch, Minneapolis, MN, USA). As a result, the coupons were free of bolts or rivets (Figure 2a). Notwithstanding all the care taken in installing the thermocouples to ensure they were all aligned at a distance of 1.5 mm and 5 mm from the coupon edges, the ones embedded within the CFRP plies suffered

Both materials were assembled with the prepreg curing cycle to bond the CFRP plies to the Ti6Al4V plaque using the TAD2-52-1E oven (Despatch, Minneapolis, MN, USA). As a result, the coupons were free of bolts or rivets (Figure 2a). Notwithstanding all the care taken in installing the thermocouples to ensure they were all aligned at a distance of 1.5 mm and 5 mm from the coupon edges, the ones embedded within the CFRP plies suffered displacements due to the curing cycle. Consequently, to determine the correct position of

allowing to measure their distance with respect to the edge (three repetitions). In order to find the optimal width of cut for which most of the thermocouples were closest to the cutting edge, the skewness related to all the coupons was estimated using the statistical Minitab® software (Minitab LLC, State College, PA, USA). The optimal widths of cut found were then a_e = 1 mm and a_e = 4.5 mm, instead of 1.5 mm and 5 mm planned initially.

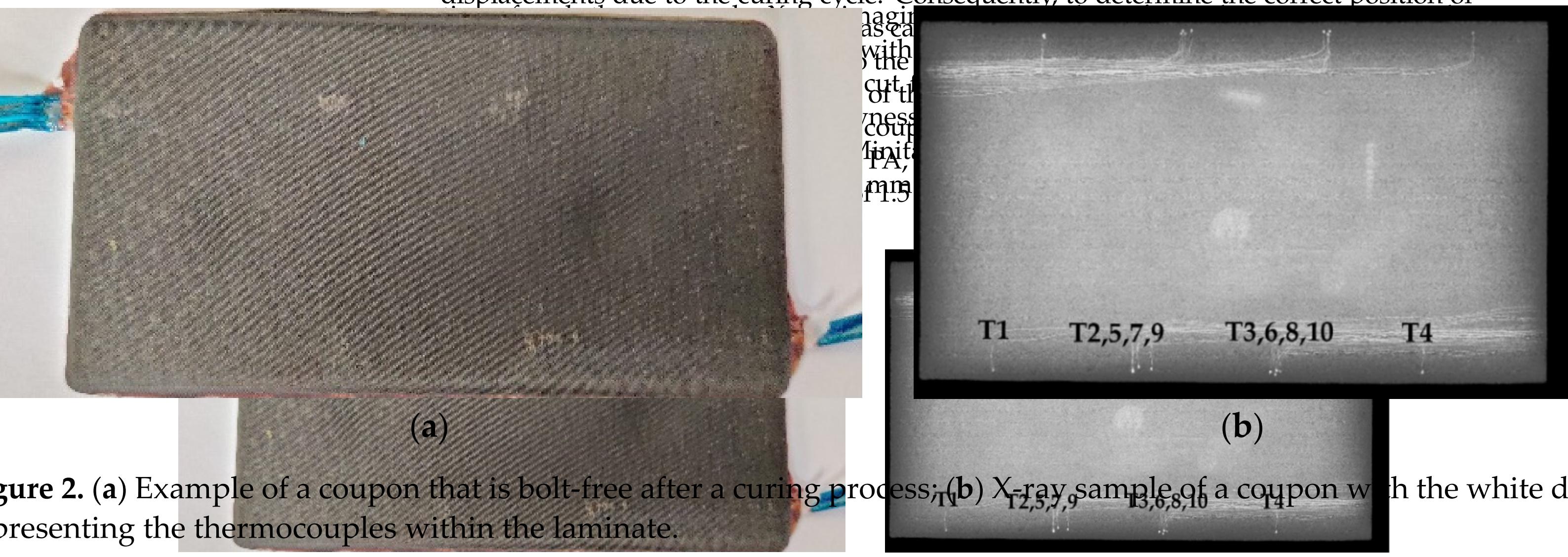

(a) (b)

Figure 2. (**a**) Example of a coupon that is bolt-free after a curing process; (**b**) X-ray sample of a coupon with the white dots representing the thermocouples within the laminate.

2.3. Experimental Setup

Figure 3 shows the machining setup used during the edge trimming of the coupons. The operation was performed using a 3-axis Huron K2X10 CNC machine tool equipped with a vacuum system for dust removal. The workpiece temperature was assessed using a Texas Instruments NI-9213 input module, having a measurement accuracy under 0.02 °C when coupled to thermocouples type K. In addition to evaluating the workpiece temperature, the temperature was also estimated close to the cutting tool edges. The tool temperature measurement was done using an M320 thermocouple measurement system connected to two thermocouples type K (accuracy of +/−1% full scale), fixed on the flutes at a 180° distance from each other. The signal was wirelessly transmitted from the tool holder to a receiver device through telemetry technology with the RF system. The signal was then converted to an analog signal corresponding to the temperature.

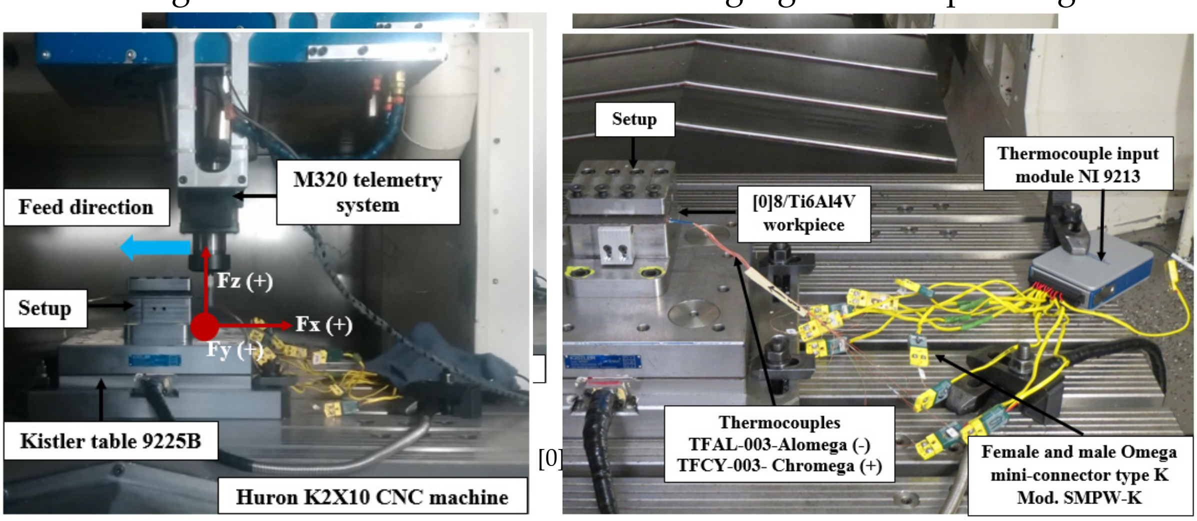

(a) (b)

Figure 3. Experimental setup for the edge trimming of [0]8/Ti6Al4V coupons: (**a**) force and cutting tool temperature acquisition system; (**b**) thermocouples arrangement.

Cutting forces were measured using a 3-axis dynamometer table (Kistler 9255B) connected to a DAQ system for recording Fx, Fy and Fz components. Besides, each experiment was performed using a new cutting section for each tool, with each section equipped with two thermocouples, as mentioned below. A total of 45 experiments were carried out using down-milling and dry cutting conditions.

2.4. Data Processing

2.4.1. Workpiece and Cutting Tool Temperature

Figure 4 shows an example of thermocouple signals from both the workpiece and the cutter. For the $[0]_8$/Ti6Al4V stack temperature, ten measurement recordings from T1 to T10 are displayed. T1 is the first in contact with the cutter. In order to find the correct position of all thermocouples, Figure 4a was correlated using the X-ray films of Figure 2b to know their exact position, the less shiny points being the welded thermocouples on the Ti6Al4V plaque. By using Yashiro's assumption [7], the closer the thermocouple tip of the cutter edge, the higher the temperature. Thus, the highest temperature within the workpiece corresponds to the thermocouple closest to the cutting area. For the cutting tool, the temperature recording is represented by T1 and T2 in Figure 4b, corresponding to both cutting tool thermocouple on each lip.

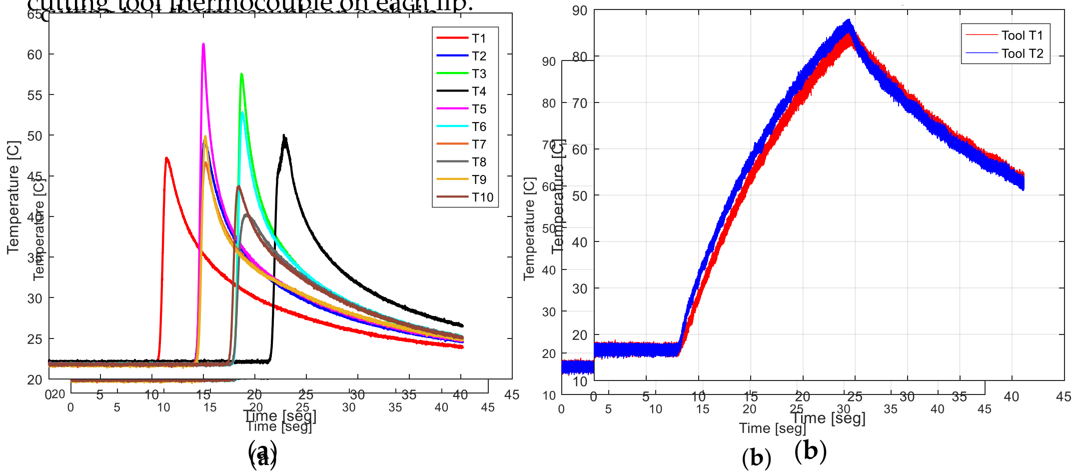

Figure 4. Examples of temperature profiles: (**a**) $[0]_8$/Ti6Al4V within stack thermocouples temperature; (**b**) cutting tool lip temperatures.

2.4.2. Cutting Forces Measurement

Figure 5 shows the layout setup of the cutting forces using the Kistler 9225B table. Figure 5a shows the direction of the forces within the $[0]_8$/Ti6Al4V stack. The forces in the X, Y, and Z directions are, respectively, the feed, normal, and axial forces. Figure 5b shows an example of a feed force signal recorded. The orange line represents the average values, calculated with Matlab software, over 30 revolutions when the force is in the steady state within the workpiece. This same method was repeated for the normal and axial forces.

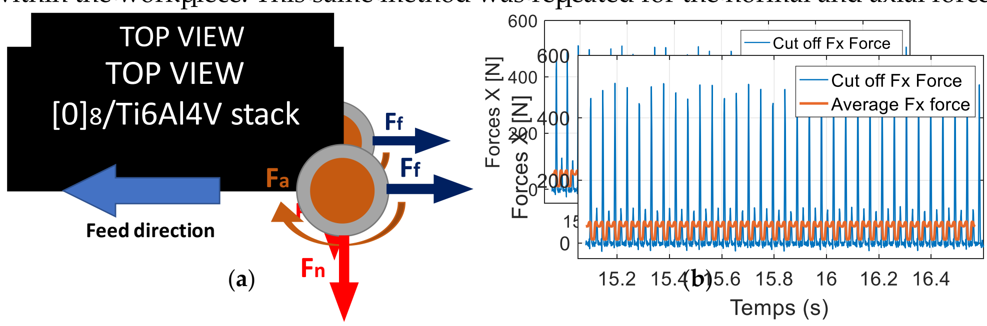

(**a**) (**b**)

Figure 5. Cutting forces setup: (**a**) force direction layout within $[0]_8$/Ti6Al4V stack; (**b**) feed force sample.

2.4.3. Roughness Evaluation on the $[0]_8$/Ti6Al4V Stack Material

The SJ400 Mitutoyo Surftest profilometer(Mitutoyo, Aurora, IL, USA) was used to measure the surface on the $[0]_8$/Ti6Al4V stack. The profilometer is equipped with a 2µm spherical diamond and is controlled by SURFPAK-SJ acquisition software. Each test profile was performed following the ISO 4287-1997 standard, and Table 3 shows the input parameters. The surface roughness parameter *Ra* was estimated once on the Ti6Al4V plaque, and twice on the $[0]_8$ plaque.

Table 3. Input parameters.

Description	Value
Sampling length	0.8 mm
Filtered Ls	2.5 µm
Evaluation length λs	16 mm
Cut-off λc	0.8 mm

2.4.4. Tool Wear

Tool wear was measured on every single flute using a Keyence VHC-500F digital microscope (Keyence, Osaka, Japan) equipped with an image processing system. The microscope has a resolution of 2 million pixels (1600 × 1200). The end of the tool life was set at 0.3 mm *VB* tool flank wear.

3. Results

All results were analyzed using Minitab and Matlab (Mathworks, Natick, MA, USA) software to observe and quantify the effects of the different cutting parameters on the measurement responses for the edge trimming of the $[0]_8$/Ti6Al4V stack.

3.1. Workpiece and Cutting Tool Temperature

3.1.1. Ti6Al4V Plaque Temperature

The average cutting temperature on thermocouple T1-2-3-4 was analyzed in terms of main effect plot. Figure 6 shows that the type of tool and the feed per tooth are the most relevant factors on the Ti6Al4V plaque temperature. Tool1 is the cutter that produced the lowest workpiece temperature, while tool2 and tool3 showed similar temperature behaviours at the surface of the Ti6Al4V. Temperature at the Ti6Al4V/CFRP interface is about 15 °C higher for both the coated carbide and PCD tools vs the uncoated carbide. The temperature difference between the carbide tools could be caused by the relatively inadequate coating for titanium machining.

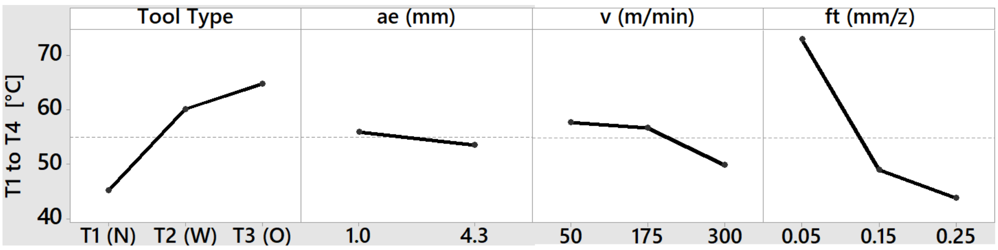

Figure 6. Main effect plot results on the Ti6Al4V plaque temperature for thermocouples T1 to T4.

Figure 6. Main effect plot results on the Ti6Al4V plaque temperature for thermocouples T1 to T4.

In the case of the feed per tooth, it greatly impacts the titanium plaque temperature. As a result, the lower the feed per tooth, the higher the Ti6Al4V/CFRP interface temperature. This is because the tool–workpiece interface engages for a longer period, with low ft causing more friction and generating more heat on the workpiece's surface. This observation differs from Yujing et al., which related the cutting speed as the main factor affecting the Ti6Al4V temperature [10].

Figure 7a shows the feed per tooth as the most significant factor, followed by the tool type-feed per tooth combination using the Response Surface Methodology (RSM). Both cutting speed and width of cut had no significant impact on the cutting temperature at the Ti6Al4V/CFRP interface. This remark confirms the previous observation. Figure 7b depicts a 3D bar plot in which a low feed per tooth significantly impacts the Ti6Al4V plaque cutting temperature. Both tool2 and tool3 have similar temperatures, while tool1 has the lowest one.

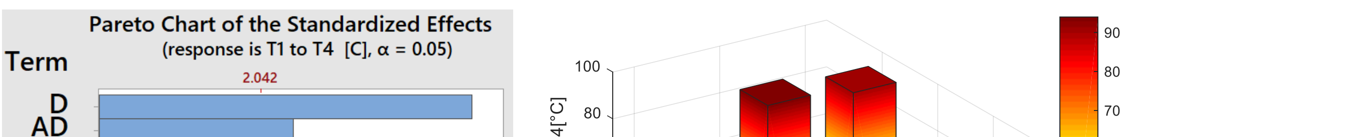

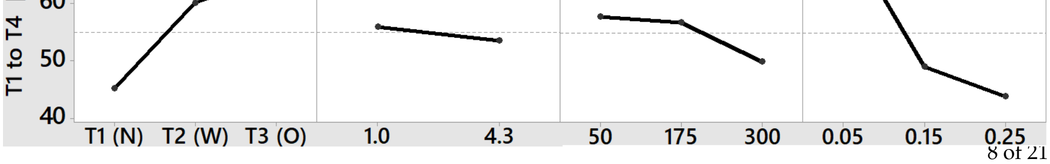

Figure 6. Main effect plot results on the Ti6Al4V plaque temperature for thermocouples T1 to T4.

Figure 7a shows the feed per tooth as the most significant factor, followed by the tool type-feed per tooth combination using the Response Surface Methodology (RSM). Both cutting speed and width of cut had no significant impact on the cutting temperature at the Ti6Al4V/CFRP interface. This remark confirms the previous observation. Figure 7b depicts a 3D bar plot in which a low feed per tooth significantly impacts the Ti6Al4V plaque cutting temperature. Both tool2 and tool3 have similar temperatures, while tool1 has the lowest one.

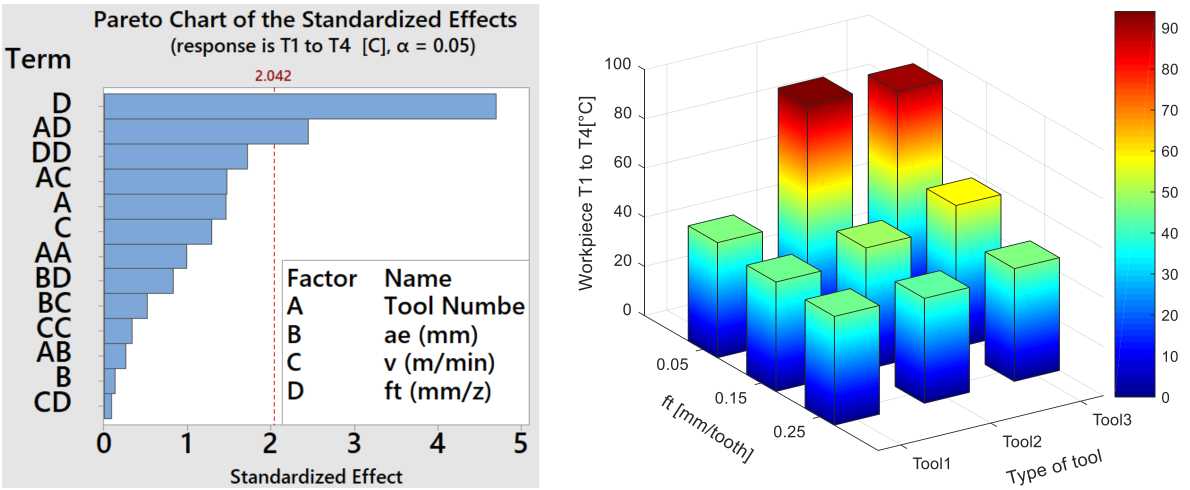

(**a**) (**b**)

Figure 7. (**a**) Pareto chart of standardized effects on T1 to T4; (**b**) 3D bar effect graph for T1 to T4.

Figure 8 shows the average Ti6Al4V plaque temperature through the longitudinal cutting length using tool2 and tool3. The 3D surface mesh results from the interpolation and extrapolation temperature as a function of the width of cut and the longitudinal cutting distance. The X-axis shows the longitudinal cutting length of the Ti6Al4V plaque, the Y-axis shows the thermocouples' position within the plaque, and the Z-axis is the temperature within the plaque. Figure 8a shows the temperature trajectory within the Ti6Al4V plaque for tool2, while Figure 8b shows the temperature for tool3. Both graphs in Figure 8 follow a linear trajectory with the highest temperature at the end of the cutting length. In the case of tool2, using the same cutting conditions, heat is transferred more rapidly to the workpiece than to tool3. This is because the thermal conductivity of tool3 is higher than that of tool2, which means the former dissipates more heat energy.

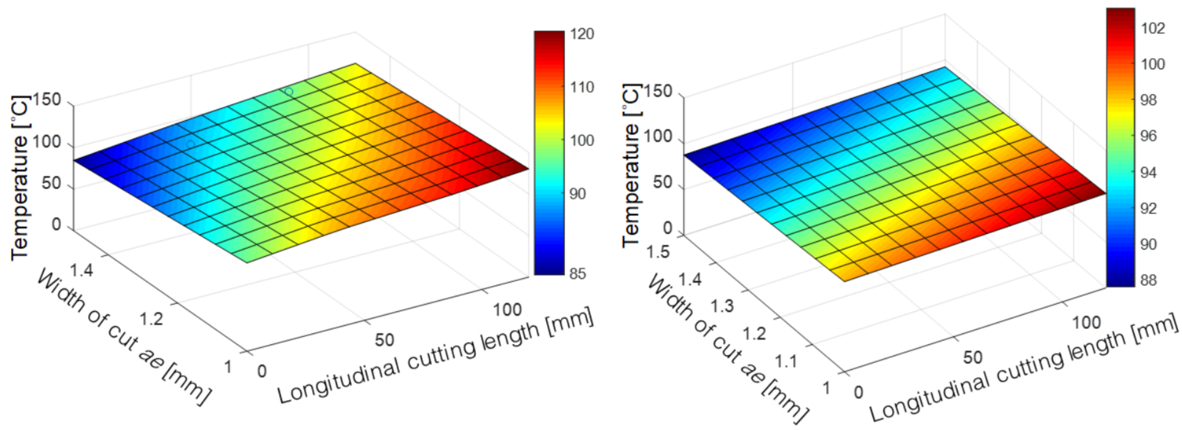

(**a**) (**b**)

Figure 8. Cutting temperature profile for the Ti6Al4V plaque for an *ft* of 0.05 mm/tooth, *v* of 175 m/min and an *ae* of 1 mm: (**a**) 3D surf mesh cutting temperature for tool2; (**b**) 3D surf mesh cutting temperature for tool3.

(a) (b)

Figure 8. Cutting temperature profile for the Ti6Al4V plaque for an *ft* of 0.05 mm/tooth, *v* of 175 m/min and an *ae* of 1 mm; (**a**) 3D surf mesh cutting temperature for tool2; (**b**) 3D surf mesh cutting temperature for tool3.

Figure 9 shows the worst possible temperature scenario during heat diffusion in the cutting process through the longitudinal direction recorded using thermocouples T1-2-3-4 (*ft* = 0.05 mm/tooth, *v* = 175 m/min, *ae* = 1 mm). The plot shows four profiles: the solid orange one represents the temperature before the cutter touches the thermocouple, the blue one represents the heat due to dissipation once the cutter passes the thermocouple, while the solid red line represents the maximum temperature recorded when the cutter touches the thermocouple. The two profiles—before and after cutting—were symmetrically plotted considering a 330 milliseconds time interval with respect to the maximum temperature (330 milliseconds) in order to observe the change of gradients within the Ti6Al4V plaque. From these profiles, as the temperature increases through the cutting length, the difference (between both profiles) passes from 5.07 °C (T1) to 23 °C (T4) in 650 milliseconds independently of the width of cut, with the Ti6Al4V being a heat source. For both red profiles, the solid red line shows the maximum temperature on each thermocouple, while the dashed line shows the worst-case interpolation temperature. Therefore, the dashed line reaches about 140 °C at the end of the cutting length in Figure 9, while the maximum temperature in Figure 8b is about 102 °C. In addition, the dashed line temperature is greater than that of the solid red line because it corresponds to the temperature near the cutting edge.

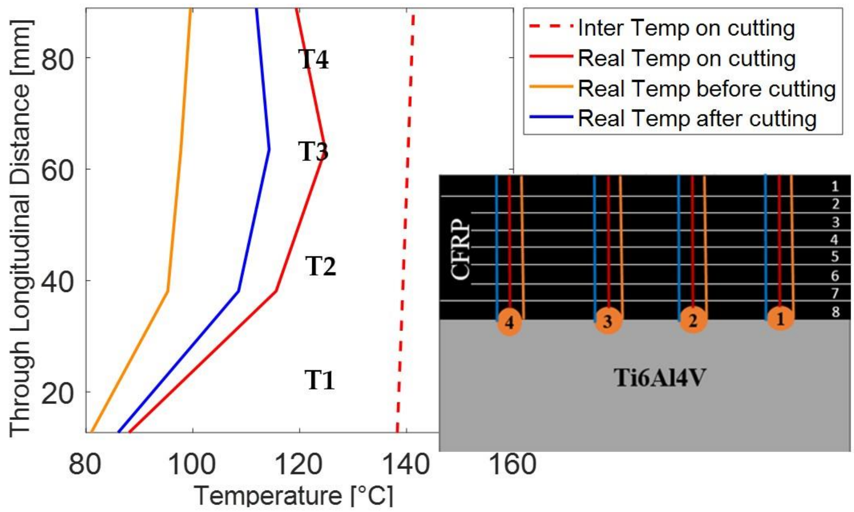

Figure 9. The temperature through the longitudinal distance for the titanium plaque using tool3, *v* of 175 m/min, *ft* of 0.05 mm/tooth, and *ae* of 1mm.

3.1.2. Composite Plaque Temperature

In the case of the thermocouples embedded within the plies of the $[0]_8$ plaque, Figure 10a shows the Pareto chart of standardized effects for thermocouples T5 to T10. As for the Ti6Al4V plaque, the feed per tooth is the most significant factor affecting the cutting temperature of the CFRP. Figure 10b shows a 3D bar plot in which a low feed per tooth significantly impacts the CFRP plaque cutting temperature. This confirms other researches examining the workpiece temperature in CFRP edge milling [9,16].

To illustrate the temperature transfer from the Ti6Al4V plaque to the $[0]_8$ plaque, Figure 11 shows the interlayer temperature according to the width of the cut *ae* and through the thickness. The X-axis is through the thickness of the stack, the Y-axis is the width of cut (position of the thermocouples within the stack), and the Z-axis is temperature. Figure 11a shows the temperature for tool2, and Figure 11b for tool3. Both figures show that the temperature decreases within the $[0]_8$ layers at different rates. The temperature decreases faster using tool2 than using tool3 in Figure 11. This might be because tool2's geometry has 4 flutes, and as such, it can dissipate more heat through the chip. In both cases, the highest temperature originates in the Ti6Al4V plaque on the cutting edge surface and decreases through the CFRP layers.

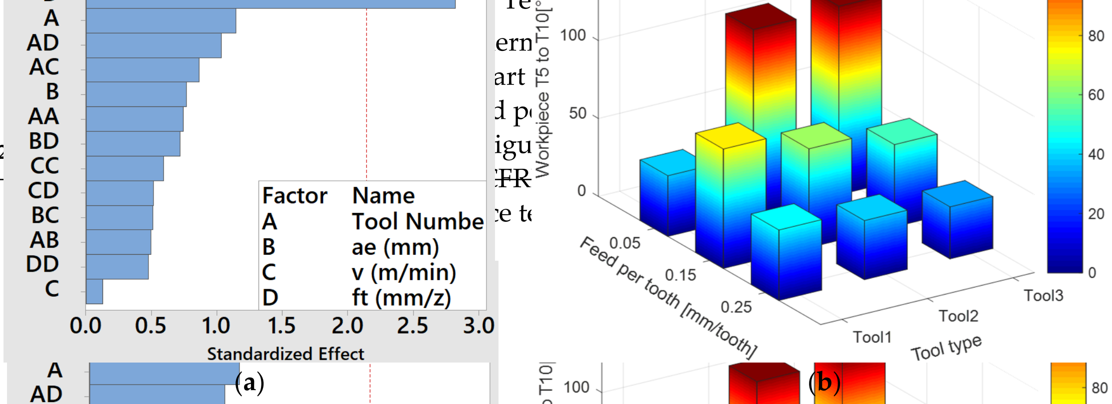

(a) (b)

Figure 10. (**a**) Pareto chart of the standardized effects for T5 to T10; (**b**) 3D bar effect graph for T1 to T4.

To illustrate the temperature transfer from the Ti6Al4V plaque to the $[0]_8$ plaque, Figure 11 shows the interlayer temperature according to the width of the cut *ae* and through the thickness. The X-axis is through the thickness of the stack, the Y-axis is the width of cut (position of the thermocouples within the stack), and the Z-axis is temperature. Figure 11a shows the temperature for tool2, and Figure 11b for tool3. Both figures show that the temperature decreases within the $[0]_8$ layers at different rates. The temperature decreases faster using tool2 than using tool3 in Figure 11. This might be because tool2's geometry has 4 flutes, and as such, it can dissipate more heat through the chip. In both cases, the highest temperature originates in the Ti6Al4V plaque on the cutting edge surface and decreases through the CFRP layers.

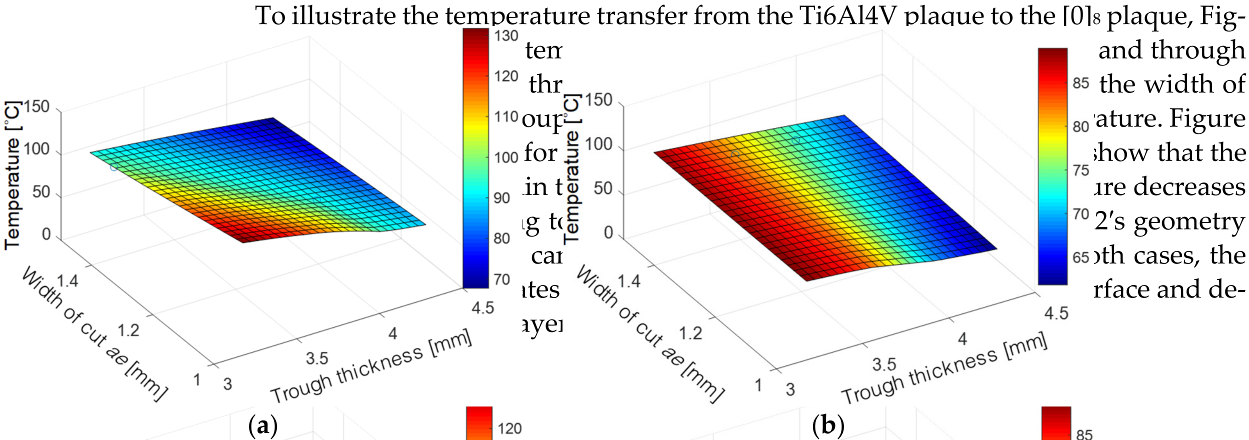

(a) (b)

Figure 11. 3D surf mesh vertical cutting temperature for thermocouples 2-5-7-9 and an *ft* of 0.05 mm/tooth, *ae* of 1 mm: (**a**) temperature trend for tool2; (**b**) temperature trend for tool3 along the stack depth.

Figure 12 shows the cutting temperature through the thickness within the $[0]_8$/Ti6Al4V stack for thermocouples T2-5-7-9 using the worst cutting conditions (v = 175 m/min, ft = 0.05 mm/tooth, ae = 1 mm). The thermocouple position is at the Y-axis through the thickness, and Figure 12 consists of 4 profiles, similar to Figure 9. The profiles before and after cutting were symmetrically plotted from the maximum temperature to show the heat dissipation from the Ti6Al4V plaque (T2) to the CFRP plaque (T5-7-9). After the temperatures of both profiles were analyzed, the heat within the Ti6Al4V plaque lasted longer than the heat within the $[0]_8$ plaque, at a ratio of about 4.5. Similar to the Ti6Al4V plaque, the solid red line shows the maximum temperature recorded by the thermocouples, while the dashed red line shows the worst case temperature interpolation. Thus, both red lines (solid and dashed lines) match in T7 since they have almost the same width of cut. In this case, thermocouple T7 has a temperature of about 115 °C, which is lower than the Tg of 190 °C for the prepreg CYCOM® 5320-1 T650-35 3K 8HS Fabric 36%. On the other hand, the dashed line temperature ranges from 155 °C at the Ti6Al4V plaque to 110 °C at T9, while Figure 11b goes from 90 °C to 60 °C.

lasted longer than the heat within the $[0]_8$ plaque, at a ratio of about 4.5. Similar to the Ti6Al4V plaque, the solid red line shows the maximum temperature recorded by the thermocouples, while the dashed red line shows the worst case temperature interpolation. Thus, both red lines (solid and dashed lines) match in T7 since they have almost the same width of cut. In this case, thermocouple T7 has a temperature of about 115 °C, which is lower than the Tg of 190 °C for the prepreg CYCOM® 5320-1 T650-35 3K 8HS Fabric 36%. On the other hand, the dashed line temperature ranges from 155 °C at the Ti6Al4V plaque to 110 °C at T9, while Figure 11b goes from 90 °C to 60 °C.

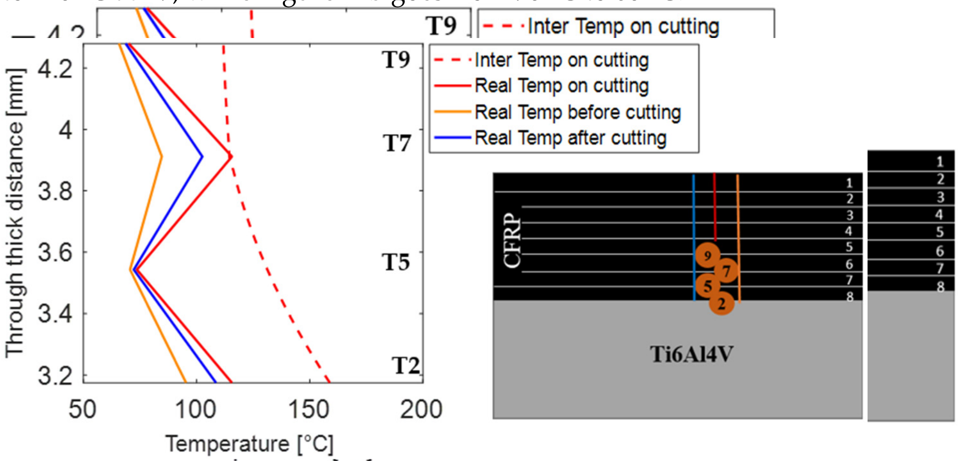

Figure 12. The temperatures T/C 2-5-7-9 along with the thickness for the $[0]_8$/Ti6Al4V stack using tool3, *v* of 175m/min, *ft* of 0.05 mm/tooth and *ae* of 1mm.

Similar to Figure 11, Figure 13 shows a temperature transfer from the Ti6Al4V plaque to the $[0]_8$ plaque, depending on the width of cut *ae* and through the thickness, for a longer cutting length (thermocouples T3-6-8-10). Therefore, there is a more significant heat transfer between layers from the Ti6Al4V plaque to the CFRP layers. Figure 13a shows the $[0]_8$/Ti6Al4V stack temperature for tool2, and Figure 13b for tool3. In addition, Figure 13 shows that the temperature decreases more rapidly by using tool2 than using tool3 (see Figure 13b). This might be because of tool2's geometry, which causes it to dissipate more heat through the chip. On the other hand, Figure 13b shows that the heat conducted within the $[0]_8$/Ti6Al4V stack is more uniform between layers. This is because tool3 can conduct more heat than the other cutters.

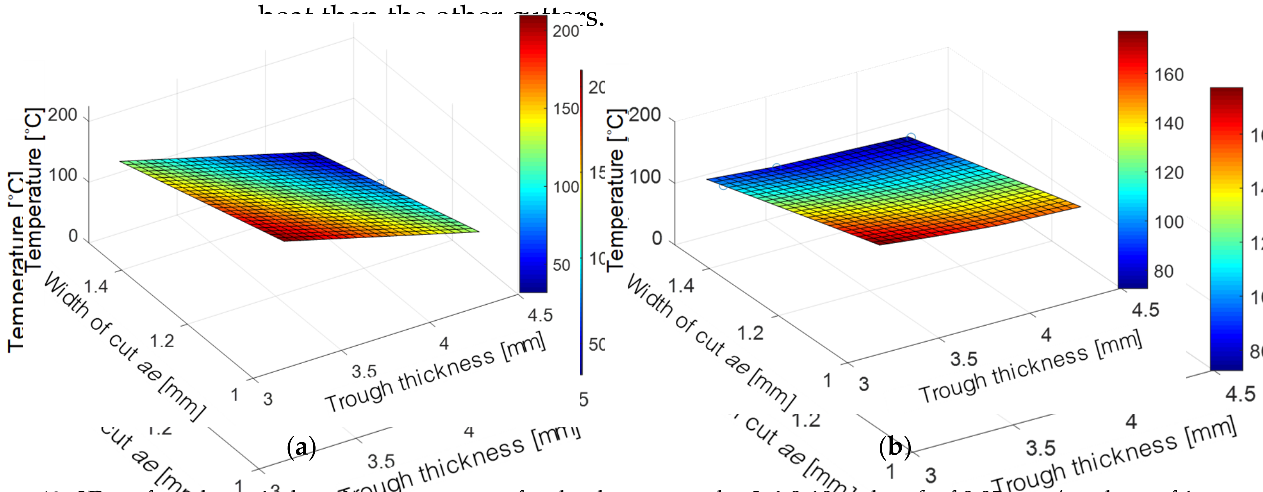

Figure 13. 3D surf mesh vertical cutting temperature for the thermocouples 3-6-8-10 and an *ft* of 0.05 mm/tooth, *ae* of 1 mm: (**a**) trend of temperature for tool2; (**b**) trend of temperature for tool3 along the stack depth.

Figure 14 shows the cutting temperature through the thickness for thermocouple T3-6-10 within the $[0]_8$/Ti6Al4V stack using the worst cutting conditions. The thermocouple is composed of four profiles, similar to Figure 12, and its position is at the Y-axis in Figure 14. The dissipation ratio decreases from 4.5 to 1.8 as the temperature cannot be dissipated through the chip. Additionally, the temperature of T6 and T10 is below the Tg.

mm: (**a**) trend of temperature for tool2; (**b**) trend of temperature for tool3 along the stack depth.

Figure 14 shows the cutting temperature through the thickness for thermocouple T3-6-10 within the $[0]_8$/Ti6Al4V stack using the worst cutting conditions. The thermocouple is composed of four profiles, similar to Figure 12, and its position is at the Y-axis in Figure 14. The dissipation ratio decreases from 4.5 to 1.8 as the temperature cannot be dissipated through the chip. Additionally, the temperature of T6 and T10 is below the Tg.

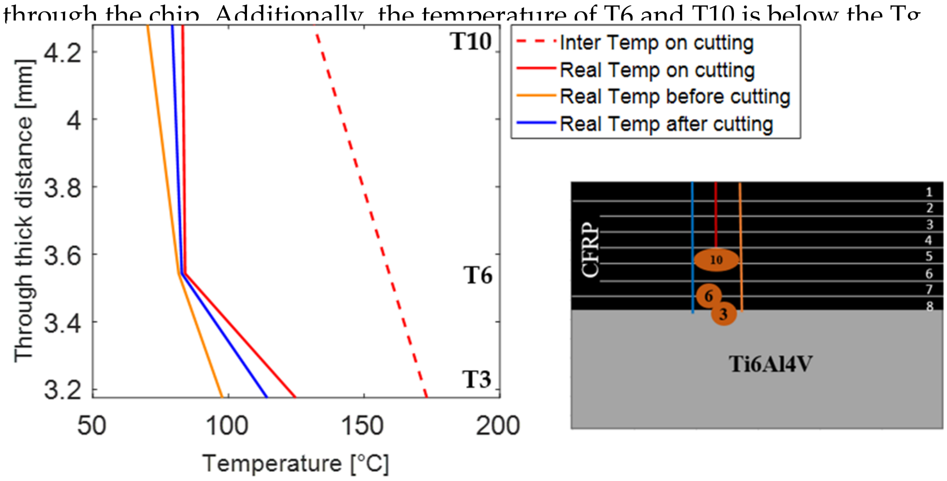

Figure 14. The temperature along the stack depth for thermocouples 3-6-10 within the $[0]_8$/Ti6Al4V stack using tool3 and cutting conditions of *v* of 175 m/min, *ft* of 0.05 mm/tooth, and *ae* of 1 mm.

3.1.3. Cutter Temperature

Figure 15 shows that tool3 (PCD material) is the cutter with the highest temperature, followed by tool2 (coated carbide TiAlN + TiAl), and finally, tool1 (uncoated carbide). In the case of tool1, sparks were observed during the experiments. This is because the cutter material fused with the Ti6Al4V plaque, and most of the heat was dissipated through the chip. As a result, tool1's temperature was lower than that of tool2 and tool3. For the radial depth of cut, the greater the *ae*, the higher the cutter temperature. Moreover, the feed per tooth has a great impact on the cutter temperature. Therefore, a low feed per tooth indicates a higher temperature since the cutter engages longer with the workpiece, producing more friction and enclosing heat in the tool–workpiece interface. On the other hand, the cutter temperature increases slightly with the cutting speed, although this is not as important as the other factors.

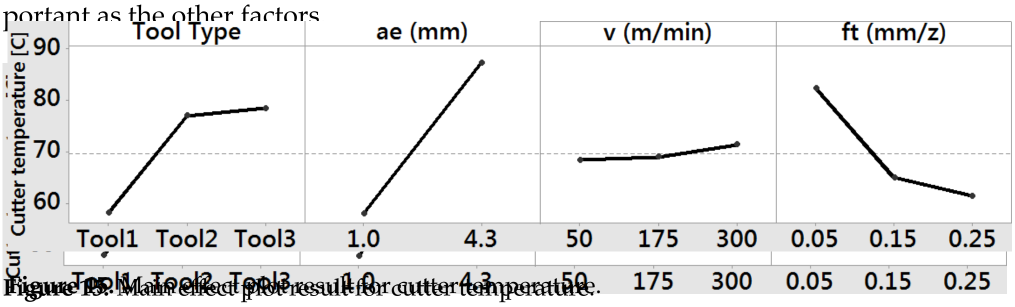

Figure 15. Main effect plot result for cutter temperature.

Figure 16a shows that the radial depth of cut is the most significant factor, followed by the type of tool, and finally, the feed per tooth according to the Pareto chart of standardized effects. Nevertheless, the cutting speed is not statistically significant, and there are no interactions between factors, unlike with the $[0]_8$/Ti6Al4V stack. Besides, Figure 16b shows that tool3 has the highest cutter temperature of all the cutters and reaches a temperature of 83.06 °C for a 1 mm radial depth of cut. In the case of a 4.3 mm radial depth of cut, tool2 reaches about 138 °C, while tool1 is about 68.91 °C, with tool2 having the highest temperature.

shows that tool3 has the highest cutter temperature of all the cutters and reaches a temperature of 83.06 °C for a 1 mm radial depth of cut. In the case of a 4.3 mm radial depth of cut, tool2 reaches about 138 °C, while tool1 is about 68.91 °C, with tool2 having the highest temperature.

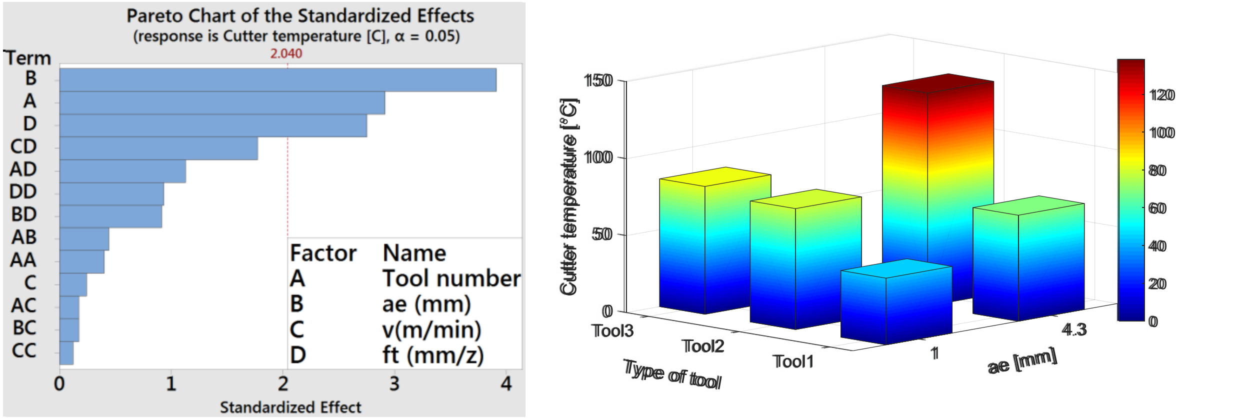

(a) (b)

Figure 16. (a) Pareto chart of the standardized effects; (b) 3D bar effect graph for the cutter temperature for an *ft* of 0.05 mm/tooth, *v* of 175 m/min.

3.2. Cutting Forces

Figure 17 shows that the radial depth of cut and the feed per tooth are the most significant factors among the cutting forces (feed, normal and axial force). Thus, the greater the radial depth of cut or the feed per tooth, the greater the force. Nevertheless, the tool type and the cutting speed have no impact on the force. In addition, the feed per tooth is the most influential factor, followed by the radial depth of cut, and finally, the interaction between them. This is in agreement with other research related to cutting forces for both CFRP and Ti6Al4V materials [11,16,25].

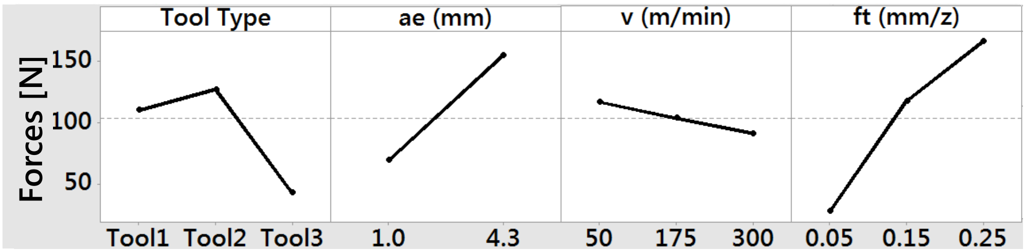

Figure 17. Main effect plot for cutting forces.

3.2.1. Feed Force

Figure 18 shows the feed force among the different cutting parameters for each cutter. The highest feed force corresponds to a high feed per tooth of 0.25 mm/tooth, a low cutting speed of 50 m/min and a high radial depth of cut of 4.3 mm. Tool1 and tool2 have a similar behaviour, although the feed force for tool2 is more significant than for tool1 for the different cutting speed values. On the other hand, tool3 has a linear trend, and the feed force increases concerning its feed per tooth, varying the cutting speeds. In addition, the feed force on tool3 is smaller than that on tool1 and tool2. This might be because tool3 is not stiff enough to cut through the titanium surface, causing tool wear and chipping under harsh cutting conditions.

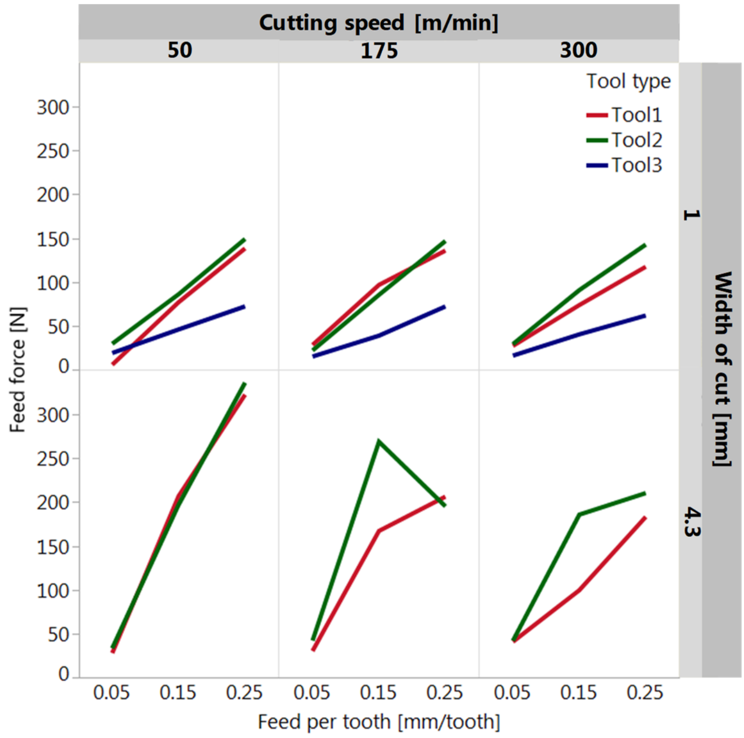

Figure 18. Feed force according to the interaction between *ft*, *v* and *ae* for each cutter.

3.2.2. Normal and Axial Forces

Both axial and normal forces show a similar trend to the feed force, in which the most significant factors are the feed per tooth and the radial depth of cut, followed by the interaction between both.

Figure 19 shows the normal and axial force according to *ft*, *v* and *ae*. Figure 19a shows the normal force for each cutter. For an *ae* of 1 mm, the normal force on tool1 is lower than on the other cutters at different cutting speed values. Both tool2 and 3 have a similar normal force trend. However, the normal force in tool3 is slightly higher than for tool2. As a result, tool3 is prone to chipping and tool wear or tool failure due to the high magnitude of the normal force and the physical proprieties of the PCD cutter. Therefore, this tool is not designed for machining the $[0]_8$/Ti6Al4V stack. For an *ae* of 4.3 mm, the normal force is 5 times greater than that for a normal force of 1 mm. The normal force for tool1 is greater than that for tool2. The greatest force magnitude of 741 N is seen for a feed of 0.25 mm/tooth and a cutting speed of 300 m/min. This is greater than any other value of the feed force or the axial force. However, for a *v* of 175 m/min and an *ae* of 4.3 mm, the trend of tool2 is different since the normal force ramps up to 576 N for an *ft* of 0.15 mm/tooth, and then decreases to 339 N for an *ft* of 0.25 mm/tooth. This might be because the chip morphology changes to extract more heat through the chips during the cutting process, turning it into a dark-bluish colour. Therefore, a second repetition could help clarify this measure.

Figure 19b shows the axial force for tool1, tool2, and tool3. For an *ae* of 1 mm, tool2 shows the highest axial force of all the cutters, while tool3 shows the lowest. The axial force of tool3 remains almost at the same magnitude for the different values of ft and v. This is due to its 2 straight flute geometry end-mill tool, which helps provide a lower axial force than for the other tools. For an *ae* of cut of 4.3 mm, tool2 (β of 35°/38°) has a higher axial force than tool1 (β of 30°). This is because tool2 has the widest helix angle. Even though the axial force is greater for tool2, it does not suffer tool wear or chipping, thanks to its protective TiAlN+TiAl coating. In addition, both tool1 and tool2 show a decrease in their axial forces for an *ft* of 0.15 to 0.25 mm/tooth and a *v* of 175 and 300 m/min. This might be because most of the heat is dissipated through the chip, changing the morphology and softening the material. Therefore, a second repetition could help clarify these measurements here as well.

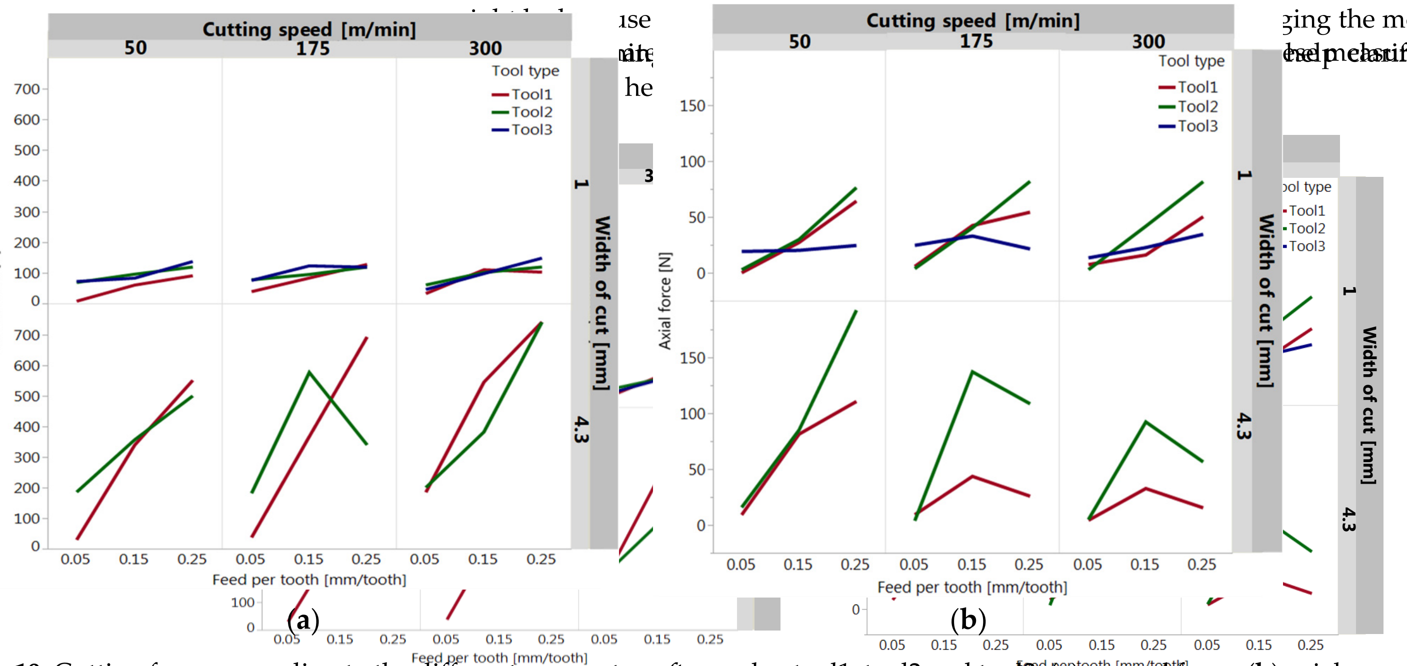

Figure 19. Cutting forces according to the different parameters: *ft*, *v* and *ae* tool1, tool2 and tool3: (**a**) normal force; (**b**) axial force.

3.3. Roughness Analysis

Figure 20 shows the arithmetic mean value (Ra) main effect analysis of the $[0]_8$/Ti6Al4V stack. Tool3 has the best performance of all the cutters, and tool1 and tool2 have a similar behaviour. For an *ae* of 4.3 mm, the greater the *ae*, the greater the roughness on the workpiece. Similar to the *ae*, when the feed per tooth is increased, the Ra increases linearly. This is opposed to the cutting speed, which decreases slightly as the cutting speed increases. Besides, the Ti6Al4V plaque presents a lower Ra than the $[0]_8$ plaque, since it is an isotropic material. Consequently, the feed per tooth is the most significant factor, followed by the workpiece material and, finally, the radial depth of cut.

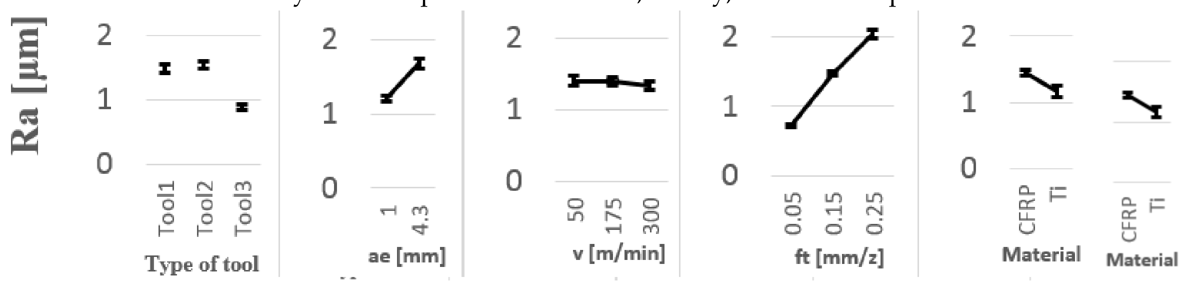

Figure 20. Ra main effect plot using ±Standard error of the mean.

In order to better understand the Ra within the CFRP and Ti6Al4V plaques, Figure 21 shows the performance of each cutter, depending on the *ft*, *v* and *ae*. Figure 21a shows the Ra within the CFRP plaque, while Figure 21b shows it within the Ti6Al4V plaque. For a 1 mm radial depth of cut in Figure 21a, tool3 has the best performance of all the cutters because it is designed for machining composite materials and its β of 0°. In the case of a 4.3 mm radial depth of cut, tool2 is slightly better than tool1, notwithstanding that both cutters are designed for machining titanium alloys. For a *v* of 50 and 175 m/min, and an *ft* of 0.15 and 0.25 mm/tooth, tool2 shows a better performance than tool1 even though tool1 has a smaller helix angle than tool2. This might be because when machining using tool1, the cutter and Ti6Al4V plaque fuse, ejecting the chip upward and damaging the CFRP plaque, unlike the case of tool2. On the other hand, Figure 21b shows the Ra on the Ti6Al4V plaque.

J. Compos. Sci. 2021, 5, x FOR PEER REVIEW 16 of 21

plaque, unlike the case of tool2. On the other hand, Figure 21b shows the Ra on the Ti6Al4V plaque. For a 1 mm radial depth of cut, the two straight flutes of tool3 show better surface roughness performance than the tool1 and tool2, even though tool3 is not designed to machine titanium alloys. Tool2 performs better than tool1. For a 4.3 mm radial depth of cut, tool2 and tool1 behave similarly for v = 50 and v = 175 m/min. As a result, tool1 performs well within this cutting range. However, tool2 performs better than tool1 for v = 300 m/min, and ft = 0.25 mm/tooth. This is because tool2 is TiAlN+TiAl coating-protected and is specially designed for machining titanium alloys in harsh conditions.

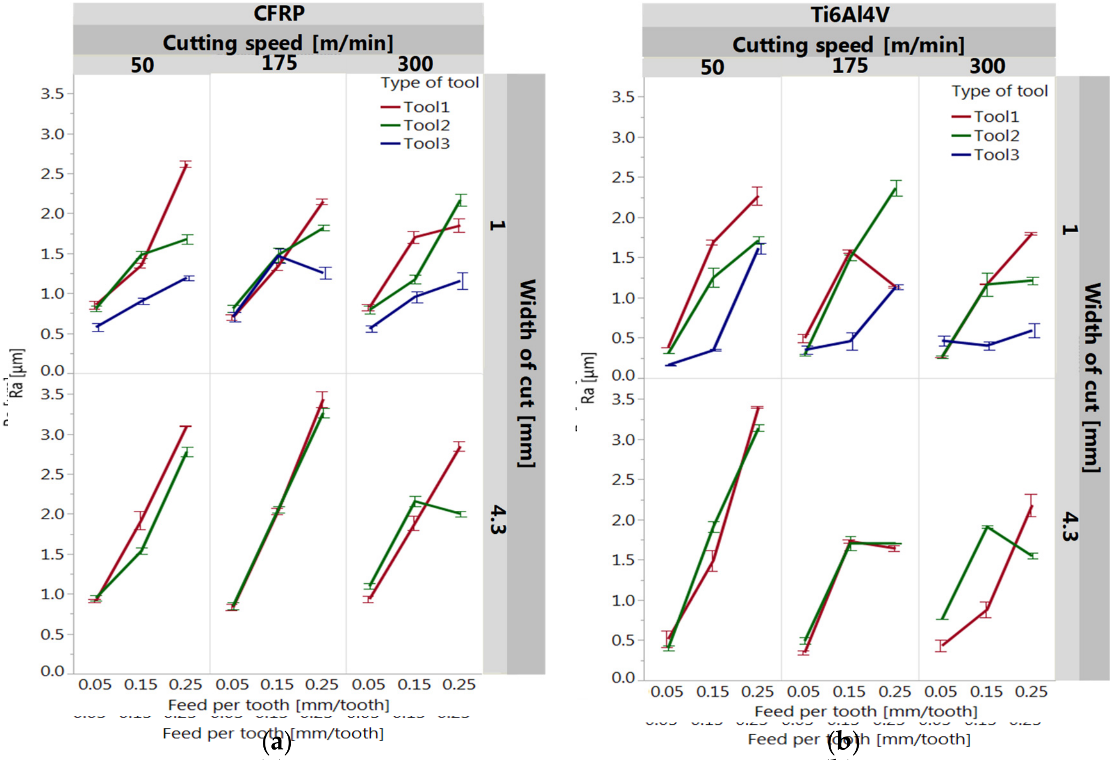

Figure 21. Arithmetic mean value (Ra) according to the different cutting parameters using ±standard error of the mean: (a) $[0]_8$ plaque; (b) Ti6Al4V plaque.

3.4. Tool Wear

Figure 22 shows that tool2 is the cutter with the lowest tool wear due to its TiAlN+TiAl coating. On the other hand, tool1 and tool3 manifest almost the same tool wear, although this main effect plot does not show the performance of the cutter using the same cutting parameters. For the radial depth of cut, the cutting speed and the feed per tooth, these three increase linearly as the magnitude increases: the higher the magnitude, the greater the wear in the cutter. Furthermore, the most significant factor is the feed per tooth, followed by the interaction between the tool type and radial depth of cut, and finally, the cutting speed.

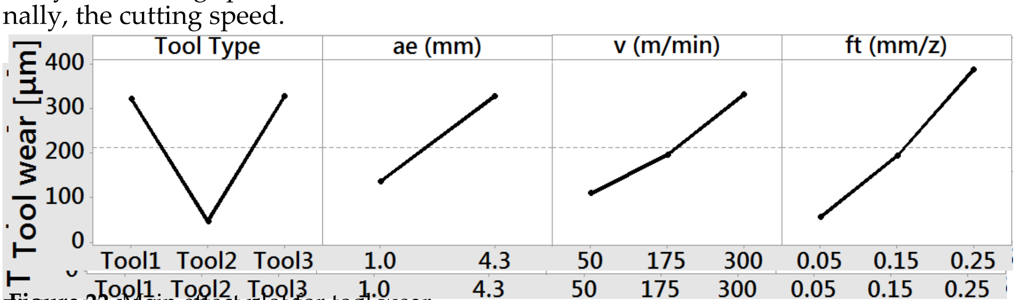

Figure 22. Main effect plot for tool wear.

J. Compos. Sci. 2021, 5, x FOR PEER REVIEW 17 of 21

Figure 23 shows the performance of each cutter using the different cutting parameters. Both tool1 and tool2 perform similarly for a 1 mm radial depth of cut. However, tool3 (PCD) is the cutter with the worst wear and is above 300 µm, which is the maximum flank wear (VB) for a *v* of 175 m/min and 300 m/min, and an *ft* of 0.25 mm/tooth. For a 4.3 mm radial depth of cut, tool2 (TiAlN+TiAl coating) is the cutter with the best performance, its tool wear being below 300 µm even in harsh conditions. This is because the tool is specially made for machining titanium alloys, although the cutter manufacturer does not recommend machining in dry conditions. On the other hand, tool1 (uncoated carbide) performs well below an *ft* of 0.15 mm/tooth and a *v* of 175 m/min. Above these parameters, its use is not recommended. Figure 24 shows the tool wear for each cutter using the worst cutting conditions. Tool1 has severe tool wear, as shown in Figure 24a. As a result, sparks were observed during the machining of the $[0]_8$/Ti6Al4V stack. This is because the tool1 material fused with the Ti6Al4V plaque due to the absence of cutting fluid. In the case of Figure 24b, tool2 does not show any chipping, flanking or fracture, even in the worst cutting conditions. Finally, Figure 24c shows that tool3 was chipped due to an excessive cutting speed and feed per tooth.

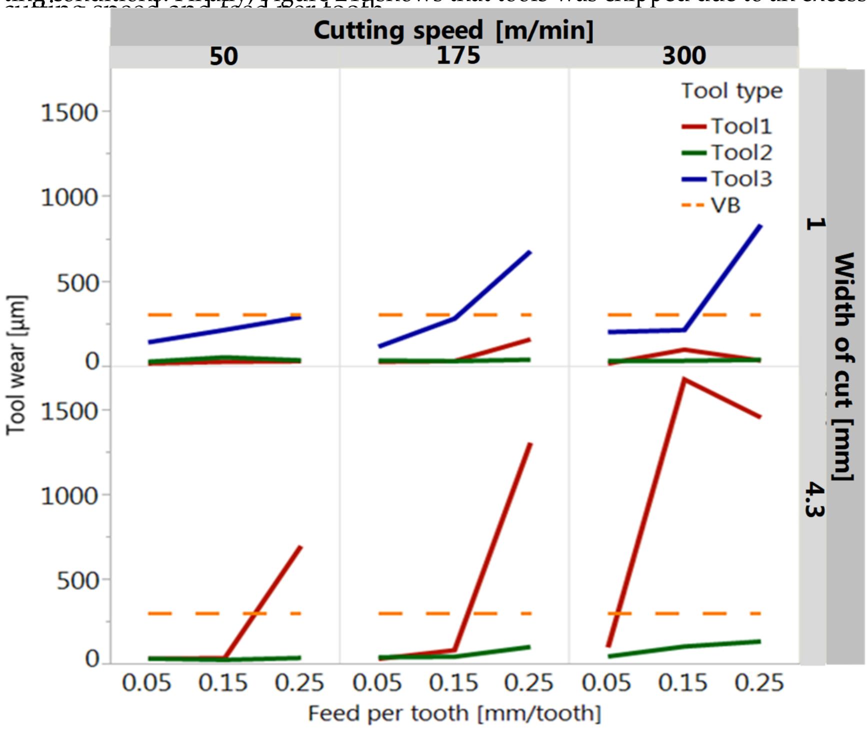

Figure 23. Tool wear effect on each cutter using the different cutting parameters.

Figure 24. Tool wear for each cutter using the worst cutting conditions: (**a**) tool1, *ae* of 4.3 mm, *v* of 300 m/min and *ft* of 0.25 mm/tooth; (**b**) tool2, *ae* of 4.3 mm, *v* of 300 m/min and *ft* of 0.25 mm/tooth; (**c**) tool3, *ae* of 1 mm, *v* of 300 m/min and *ft* of 0.25 mm/tooth.

4. Discussion

The test analysis suggests that the feed per tooth and the tool type are the factors that most influence the Ti6Al4V temperature plaque. This is contrary to the research of Y. Sun et al. and Yujing et al. [10,27], where studies found that the most relevant factor is the cutting speed, followed by the feed per tooth. This difference is due to the method used to estimate the cutting tool's temperature as well as within the workpiece in both studies. In addition, their method fails to show whether the semi-artificial thermocouple can measure the temperature in both the workpiece and the cutting tool. Therein, the temperature measurement is not mentioned (location at the tool tip, or the workpiece or both). Additionally, we found that tool3 dissipates more heat through its core than does tool2. As a result, the Ti6Al4V plaque is cooler using tool3 than by machining with the other cutters. It is worth noting that both our experiments and those of Yujing et al. [10] were carried out under dry conditions and in a down-milling cutting mode.

In the case of the $[0]_8$ plaque, the feed per tooth has the most significant effect on the temperature. Similar results were found by Kerrigan et al. and Sheikh-Ahmad et al. [9,16], but the results diverge from those of Wang et al. [7,11,12]. This may be because Wang et al. followed the same methodology as Yujing et al. [10], using a semi-artificial thermocouple. Consequently, it is hard to know if their tool–workpiece thermocouple method was estimated within the cutting tool or the workpiece since there is no physical thermocouple on the cutting edge surface. Therefore, it is difficult to assess how their semi-artificial thermocouple method, similar to a metal sheet, was able to measure the temperature of both the cutter and workpiece. In Yashiro et al. [7], the feed per tooth was constant throughout the experiments, and its effect on the temperature cutting process could not be evaluated. On the other hand, Kerrigan's results [16] showed that 60% of the energy within the workpiece is due to the feed rate. However, the energy calculated was based on cutting force data and was not compared to the measurements from their thermal camera. More recently, Sheikh-Ahamad et al. [9] studied the thermal aspects of CFRP machining and the effects of the cutting tool type and cutting parameters. Sheikh-Ahamad's results showed that the feed per tooth is the most significant factor. This is because the cutter moves forward faster through the workpiece. As a result, the heat retention in the workpiece is lower than in the context of a low feed per tooth, which is in agreement with our results. Finally, both Sheikh-Ahmad [9] and the present study report that the cutting speed is not a significant factor behind temperature variations within the workpiece.

Several studies have reported on the tool temperature measurement for the cutting tool temperature using different techniques, although only a few of them have obtained relevant results. In Yashiro et al. [7], thermal cameras could not assess the tool temperature since the heat radiation saturates the thermography at the cutting point location. On the other hand, Yujing et al. [10] estimated the cutter temperature using a semi-artificial thermocouple within the workpiece. Their statistical analysis shows that the cutter temperature has the same cutting speed trend as the workpiece, which is the most significant factor, followed by the feed per tooth, and finally, the radial depth of cut. Yujing's results [10] are different from those of Kerrigan's [16] in that the radial depth of cut is the most significant factor in the former study. This difference is due to the different methods used to measure the cutting edge temperature (semi-artificial thermocouple in Yujing et al. vs. a telemetry system for cutting tool thermocouples for Kerrigan et al. [16] and in the present study). Moreover, Sheikh-Ahmad et al. [9] reported that neither the cutting speed nor the feed per tooth is a significant factor, which is contrary to the findings of Yujing [10]. Because the radial depth of cut was always kept constant in Sheikh-Ahmad's DoE [9], our results can therefore not be directly compared with their results. Finally, Sheikh-Ahmad et al. [9] also studied the effects of the cutter's physical properties (geometry and material) on the temperature of the cutter, the chip, and the workpiece. However, their results for both the cutter and the workpiece showed a higher temperature than ours. This is because their CFRP cutting length is 5 times longer than ours, even when we machined the plate under dry conditions. It is worth mentioning that our study was limited to the measurement of the cutter and workpiece temperatures, as opposed to Sheikh-Ahmad et al.'s [9], which also covered the chip temperature.

Concerning the cutting forces, the feed per tooth has the most influence on the feed, normal and axial forces for the $[0]_8$/Ti6Al4V stack. For the cutting forces on the Ti6Al4V plaque, Jinyang et al. and Xu et al. [5,6] noted that the cutting force "Fy" is greater than the thrust force "Fx" in the orthogonal cutting process of the $[0]_8$/Ti6Al4V stack as reported in this research. However, their machining proceeded from CFRP to Ti6Al4V or vice-versa and did not involve both materials simultaneously. Moreover, their analysis was based on the cutting speed, the fiber orientation and the depth of cut, with the feed per tooth excluded. On the other hand, Yujing et al. [10] measured the cutting forces and observed a correlation with the temperature recorded within the titanium workpiece. Their results show that the force and temperature vary in parallel and complement each other. In addition, their study was based on determining the most relevant factor impacting the temperature generated during the machining while excluding the most significant factors in the cutting forces, which is why our results cannot be compared with those relating to their titanium plaques.

Concerning the CFRP cutting forces, our results were similar to those of Haijin et al. and Kerrigan et al. [11,16]. In Kerrigan et al. [16], their results consider the resultant force composed of Fx, Fy, and Fz. On the other hand, Haijin's cutting results [11] show the resulting cutting force between the Fx and Fy. Both works show that the feed per tooth is the most significant factor for the CFRP plaque. However, the results are not conclusive because the plastic deformation force of the titanium plaque is greater than the brittle fracture force of the CFRP plaque. Consequently, the plastic deformation of the titanium material in the $[0]_8$/Ti6Al4V plaque is the most influential factor affecting the cutting force.

For the roughness parameter Ra, the feed per tooth is the most significant factor, which increases with an increase in the feed per tooth, and decreases slightly with an increase in the cutting speed for both the CFRP and Ti6Al4V plaques. As a result, a low feed per tooth, a high cutting speed and a low radial depth of cut are recommended to reduce the average surface roughness. In the case of the CFRP material, the result is consistent with that of Chatelain et al. [28], in which the feed per tooth has the most significant effect. On the other hand, for the titanium, Yang et al. [30] suggest a low feed per tooth and a low radial depth of cut and a high cutting speed, as is suggested in this study. A similar action on parameters could be used to achieve a smoother surface finish during the machining of the $[0]_8$/Ti6Al4V stack.

5. Conclusions

Combinations of different cutting parameters (cutting speed, radial depth of cut, and feed per tooth) and tool types were assessed using the tool–workpiece thermocouple method to measure the cutting temperature both on the cutter and within the $[0]_8$/Ti6Al4V stack. In addition, the cutting forces, the roughness and the tool wear during the edge milling cutting process were evaluated. We found that the feed factor is the most significant factor affecting the cutting temperature for the CFRP and Ti plaques, instead of the cutting speed. Therefore, the temperature of the workpiece increases when decreasing the feed per tooth and decreases when increasing the cutting speed; however, the latter is not as significant as the feed per tooth. For the radial depth of cut, this factor is not as significant in the $[0]_8$/Ti6Al4V stack temperature as it is in the cutter temperature. Therefore, in order to increase the workpiece machining efficiency, this research recommends using tool2 (coated TiAlN+TiAl). This is because it showed the lowest wear of the three cutters tested, the other two being tool1 (uncoated tool) and tool3 (PCD tool), and because it did not fuse with the Ti6Al4V alloys as did tool1, or chip like tool3.

In addition, the tool–workpiece thermocouple method showed that even a few tenths of millimeters could change the temperature within the $[0]_8$/Ti6Al4V stack. This is due to the displacement of the thermocouples within the CFRP plaque during the curing process. Moreover, due to the size of the $[0]_8$/Ti6Al4V stack, the workpiece and cutter temperatures increase along the cutting length. Thus, future work is to set a numerical model in order to predict the temperature for real size parts using the experimental data obtained from this research.

For the cutting forces, the highest force is in the normal direction, and it increases as the feed per tooth is increased, contrary to the $[0]_8$/Ti6Al4V stack temperature, which decreases under the same circumstance (increased feed per tooth). Therefore, the temperature and normal force have inversely proportional magnitudes. Additionally, in order to reduce the surface roughness (Ra) resulting from the edge milling of the CFRP/Ti6Al4V stack, it is recommended to use a low feed per tooth and radial depth of cut and a high cutting speed in order to compensate for the temperature within the CFRP plaque.

Author Contributions: Conceptualization and methodology design, A.C.-M., J.-F.C. and G.L.; Experiments, A.C.-M.; Data analysis and validation, A.C.-M., J.-F.C., G.L. and X.R.; Software, A.C.-M.; Writing—original draft preparation, A.C.-M., J.-F.C. and X.R.; writing—Review and editing, A.C.-M., J.-F.C. and X.R.; supervision, J.-F.C. and G.L.; project administration, J.-F.C. All authors have read and agreed to the published version of the manuscript.

Funding: This research was partly financed by NSERC RGPIN-2017-04305.

Acknowledgments: The authors are grateful for the scholarship support of A.C. provided by the Consejo Nacional de Ciencia y Tecnología (CONACYT) and by the Consejo Potosino de Ciencia y Tecnologia (COPOCYT) through scholarship (No. 410615).

Conflicts of Interest: The authors declare no conflict of interest.

References

1. Xu, J.; Mkaddem, A.; El Mansori, M. Recent advances in drilling hybrid FRP/Ti composite: A state-of-the-art review. *Compos. Struct.* **2016**, *135*, 316–338. [CrossRef]
2. SenthilKumar, M.; Prabukarthi, A.; Krishnaraj, V. Study on Tool Wear and Chip Formation During Drilling Carbon Fiber Reinforced Polymer (CFRP)/Titanium Alloy (Ti6Al4V) Stacks. *Procedia Eng.* **2013**, *64*, 582–592. [CrossRef]
3. BBrinksmeier, E.; Fangmann, S.; Rentsch, R. Drilling of composites and resulting surface integrity. *Cirp Ann. Manuf. Technol.* **2011**, *60*, 57–60. [CrossRef]
4. Park, K.-H.; Beal, A.; Kim, D. A Comparative Study of Carbide Tools in Drilling of CFRP and CFRP-Ti Stacks. *J. Manuf. Sci. Eng.* **2013**, *136*, 014501. [CrossRef]
5. Jinyang, X.; El Mansori, M. An experimental investigation on orthogonal cutting of hybrid CFRP/Ti stacks. In Proceedings of the ESAFORM 2016: 19th International ESAFORM Conference on Material Forming, Nantes, France, 27–29 April 2016; AIP—American Institute of Physics: New York, NY, USA, 2016.
6. Xu, J.; El Mansori, M.; Chen, M.; Ren, F. Orthogonal cutting mechanisms of CFRP/Ti6Al4V stacks. *Int. J. Adv. Manuf. Technol.* **2019**, *103*, 3831–3851. [CrossRef]
7. Yashiro, T.; Ogawa, T.; Sasahara, H. Temperature measurement of cutting tool and machined surface layer in milling of CFRP. *Int. J. Mach. Tools Manuf.* **2013**, *70*, 63–69. [CrossRef]
8. Pan, W.; Kamaruddin, A.; Ding, S.; Mo, J. Experimental investigation of end milling of titanium alloys with polycrystalline diamond tools. *Proc. Inst. Mech. Eng. Part B J. Eng. Manuf.* **2014**, *228*, 832–844. [CrossRef]
9. Sheikh-Ahmad, J.; Almaskari, F.; Hafeez, F. Thermal aspects in machining CFRPs: Effect of cutter type and cutting parameters. *Int. J. Adv. Manuf. Technol.* **2018**, *100*, 2569–2582. [CrossRef]
10. Yujing, S.; Jie, S.; Jianfeng, L. An experimental investigation of the influence of cutting parameters on cutting temperature in milling Ti6Al4V by applying semi-artificial thermocouple. *Int. J. Adv. Manuf. Technol.* **2014**, *70*, 765–773.
11. Wang, H.; Sun, J.; Li, J. Evaluation of cutting force and cutting temperature in milling carbon fiber-reinforced polymer composites. *Int. J. Adv. Manuf. Technol.* **2016**, *82*, 1517–1525. [CrossRef]
12. Wang, H.; Sun, J.; Zhang, D. The effect of cutting temperature in milling of carbon fiber reinforced polymer composites. *Compos. Part. A Appl. Sci. Manuf.* **2016**, *91*, 380–387. [CrossRef]
13. Li, L.; Chang, H.; Wang, M.; Zuo, D.W.; He, L. Temperature measurement in high speed milling Ti6Al4V. *Key Eng. Mater.* **2004**, *259*, 804–808. [CrossRef]
14. Delahaigue, J.; Chatelain, J.-F.; Lebrun, G. Influence of Cutting Temperature on the Tensile Strength of a Carbon Fiber-Reinforced Polymer. *Fibers* **2017**, *5*, 46. [CrossRef]
15. Ghafarizadeh, S.; Lebrun, G.; Chatelain, J.-F. Experimental investigation of the cutting temperature and surface quality during milling of unidirectional carbon fiber reinforced plastic. *J. Compos. Mater.* **2016**, *50*, 1059–1071. [CrossRef]
16. Kerrigan, K.; O'Donnell, G.E. On the Relationship between Cutting Temperature and Workpiece Polymer Degradation During CFRP Edge Trimming. *Procedia Cirp* **2016**, *55*, 170–175. [CrossRef]

17. Kerrigan, K.; Thil, J.; Hewison, R. An integrated telemetric thermocouple sensor for process monitoring of CFRP milling operations. In Proceedings of the 5th CIRP Conference on High Performance Cutting 2012, HPC 2012, Zurich, Switzerland, 4–7 June 2012; Elsevier: Zurich, Switzerland, 2012.
18. Le Coz, G.; Marinescu, M.; Devillez, A.; Dudzinski, D.; Velnom, L. Measuring temperature of rotating cutting tools: Application to MQL drilling and dry milling of aerospace alloys. *Appl. Therm. Eng.* **2012**, *36*, 434–441. [CrossRef]
19. Wu, H.B.; Zhang, S.J. 3D FEM simulation of milling process for titanium alloy Ti6Al4V. *Int. J. Adv. Manuf. Technol.* **2014**, *71*, 1319–1326. [CrossRef]
20. Ducobu, F.; Rivière-Lorphèvre, E. Material constitutive model and chip separation criterion influence on the modeling of Ti6Al4V machining with experimental validation in strictly orthogonal cutting condition. *Int. J. Mech. Sci.* **2016**, *107*, 136–149. [CrossRef]
21. Santiuste, C.; Díaz-Álvarez, J.; Soldani, X.; Miguélez, H. Modelling thermal effects in machining of carbon fiber reinforced polymer composites. *J. Reinf. Plast. Compos.* **2014**, *33*, 758–766. [CrossRef]
22. Yang, Y.; Zhu, W. Study on cutting temperature during milling of titanium alloy based on FEM and experiment. *Int. J. Adv. Manuf. Technol.* **2014**, *73*, 1511–1521. [CrossRef]
23. Sui, S.; Feng, P. Investigation on generation and features of burn defect in Ti6Al4V milling. *Int. J. Adv. Manuf. Technol.* **2016**, *87*, 949–955. [CrossRef]
24. Nemetz, A.W.; Daves, W.; Klünsner, T.; Praetzas, C.; Liu, W.; Teppernegg, T.; Czettl, C.; Haas, F.; Bölling, C.; Schäfer, J. Experimentally validated calculation of the cutting edge temperature during dry milling of Ti6Al4V. *J. Mater. Process. Technol.* **2020**, *278*, 116544. [CrossRef]
25. Wu, H.; Zhang, S. Effects of cutting conditions on the milling process of titanium alloy Ti6Al4V. *Int. J. Adv. Manuf. Technol.* **2015**, *77*, 2235–2240. [CrossRef]
26. Pan, W.; Ding, S.; Mo, J. Thermal characteristics in milling Ti6Al4V with polycrystalline diamond tools. *Int. J. Adv. Manuf. Technol.* **2014**, *75*, 1077–1087. [CrossRef]
27. Sun, Y.; Sun, J.; Li, J. Modeling and experimental study of temperature distributions in end milling Ti6Al4V with solid carbide tool. *Proc. Inst. Mech. Eng. Part. B J. Eng. Manuf.* **2017**, *231*, 217–227. [CrossRef]
28. Chatelain, J.F.; Zaghbani, I.; Monier, J. Effect of Ply Orientation on Roughness for the Trimming Process of CFRP Laminates. *Int. J. Ind. Manuf. Eng.* **2012**, *6*, 1516–1522.
29. Luo, B.; Li, Y.; Zhang, K.; Cheng, H.; Liu, S. A novel prediction model for thrust force and torque in drilling interface region of CFRP/Ti stacks. *Int. J. Adv. Manuf. Technol.* **2015**, *81*, 1497–1508. [CrossRef]
30. Yang, D.; Liu, Z. Surface topography analysis and cutting parameters optimization for peripheral milling titanium alloy Ti–6Al–4V. *Int. J. Refract. Hard Met.* **2015**, *51*, 192–200. [CrossRef]